

Advances and applications of the digital mask technique in particle image velocimetry experiments

L Gui¹, S T Wereley² and Y H Kim³

¹ NCPA, University of Mississippi, University, MS 38677-1848, USA

² Mechanical Engineering, Purdue University, West Lafayette, IN 47907-1288, USA

³ Department of Mechanical Engineering, Pohang University of Science and Technology, San 31, Hyoja-dong, Pohang 790-784, Korea

Received 14 February 2003, in final form 1 July 2003, accepted for publication 1 August 2003

Published 2 September 2003

Online at stacks.iop.org/MST/14/1820

Abstract

Some advancements of the digital mask technique, which was first described by Gui and Merzkirch (1996a *ERCOFTAC Bull.* **30** 45–8) for a phase-separated evaluation of two-phase flow particle image velocimetry (PIV) recordings, are presented in this paper. The originally minimum-quadratic-difference- (MQD-) based mask technique is accelerated by using the fast Fourier transformation algorithm. In order to further increase the evaluation speed and the measurement accuracy, the digital mask technique is modified so that it can be combined with the correlation-based central difference image correction (CDIC) method, which is proved to be a more accurate and less peak-locked evaluation algorithm than both the MQD tracking method and the correlation-based tracking method. An ellipse-shaped interrogation window is constructed with the digital mask technique to improve the spatial resolution of the evaluation without loss of the evaluation accuracy. Applications in PIV measurements of solid/water two-phase flow, bubbly water flow, flow around a human blood cell and airflow near the tip of a vibrating cantilever demonstrate that the combination of the digital mask technique, the CDIC algorithm and the ellipse interrogation window makes a powerful tool for evaluating digital PIV recordings of complex flows.

Keywords: fluid flow velocity, PIV, CDIC, digital mask, eclipse window, multi-phase flow, blood cell, vibrating cantilever

1. Introduction

The digital mask technique was first described by Gui and Merzkirch (1996a) for a phase-separated evaluation of particle image velocimetry (PIV) recordings for two-phase flows. It has successively been applied in PIV measurements of solid-particle/water and bubble/water two-phase flows (Hilgers *et al* 1995, Merzkirch *et al* 1997, Gui *et al* 1997, Lindken *et al* 1999, Lindken and Merzkirch 1999, 2000). Originally, the digital mask technique was introduced on the basis of the minimum-quadratic-difference (MQD) method, which is an algorithm

for tracking the pattern of particle images in the interrogation window (Gui and Merzkirch 1996b). In comparison with the conventional correlation-based interrogation algorithm, it is unbiased and its evaluation error is not dependent on the integer portion of the particle image displacement. It also works better than the correlation-based tracking algorithm in the cases of low particle image number density, small interrogation window and large particle image size (Gui and Merzkirch 2000). Before using the fast Fourier transformation (FFT) algorithm to accelerate the MQD tracking method (Gui *et al* 1998), the digital mask technique was combined with the

minimum-absolute-difference (MAD) tracking method for a fast computation (Gui and Merzkirch 1997). Although the MQD method has excellent performance for evaluating PIV recordings with ideal particle images, it is sensitive to noise added to the PIV recording. Especially in the single-exposure PIV recording pairs acquired with recent commercial PIV systems using high-resolution charge-coupled device (CCD) cameras, the brightness of particle images is obviously different between the two recordings in a pair. Therefore, the advantages of the MQD method sometimes cannot be observed very clearly for evaluating real PIV recordings. In addition, even though the MQD method can be highly accelerated with the FFT algorithm, its evaluation speed is still much lower than the FFT-accelerated, correlation-based interrogation algorithm. In the present work the authors try to further improve the performance of the digital mask technique by combining it with the correlation-based evaluation schemes.

In the past decade, several novel techniques were added to the correlation-based schemes to highly improve the accuracy of the digital PIV recording evaluation. At first, an adaptive discrete window shift technique named forward difference interrogation (FDI) was widely used with the correlation-based interrogation algorithm to reduce the evaluation error, and with the correlation-based tracking algorithm to increase the spatial resolution (Keane and Adrian 1993, Willert 1996, Cowen and Monismith 1997, Westerweel *et al* 1997). To avoid bias errors that may result from FDI in cases of curvature flow and high velocity gradient flow, another adaptive discrete window shift technique, i.e. central difference interrogation (CDI), was initially introduced by Wereley *et al* (1998) and further developed and explored by Wereley and Meinhart (2000, 2001). Continuous window shift techniques were applied for further reducing the bias and random evaluation errors and the peak-locking effect of the correlation-based interrogation algorithm (Sjödahl 1994, Sholl and Savas 1997, Gui and Wereley 2002). To account for the distortion of PIV image patterns in complex flow measurements, an image correction technique was applied with the correlation-based tracking algorithm (Huang *et al* 1993). A faster and more accurate image correction scheme named central difference image correction (CDIC) was recently introduced by Wereley and Gui (2001, 2003) in combination with the correlation-based interrogation algorithm.

In the present work we shall briefly review the MQD-based digital mask technique, describe a method for accelerating the computation and extend the digital mask technique to the correlation-based schemes. Then the evaluation uncertainties of the MQD method and three different correlation-based evaluation schemes are compared in the cases with random background noise and illumination difference between two recordings in a single-exposure PIV recording pair. As a special extension of the digital mask technique, an ellipse interrogation window is described and discussed. Finally, the CDIC-based digital mask technique with elliptical- (round-) shaped interrogation window is applied in PIV measurements of the solid/water two-phase flow, bubbly water flow, flow around a blood cell and airflow near the tip of a vibrating cantilever.

2. Description and discussion of the methods

2.1. Digital mask technique

The digital mask technique was described by Gui and Merzkirch (1996a) for a phase-separated evaluation of PIV recordings of two-phase flow on the basis of the MQD method (Gui and Merzkirch 1996b, 2000). The MQD method requires searching for the minimum of the quadratic difference

$$D(m, n) = \frac{1}{MN} \sum_{i=1}^M \sum_{j=1}^N [g_1(i, j) - g_2(i + m, j + n)]^2 \quad (1)$$

in order to determine the displacement (m^*, n^*) experienced by an ensemble of particle images during a time interval Δt . The ensemble is a 'pattern' or window of size $M \times N$ pixels in the digital PIV recording. We assume here that two consecutive single exposures, separated by the time interval Δt , are taken; g_1 and g_2 are the grey values of the pixels in the two exposures, respectively. When measuring a multi-phase flow or one-phase flow with complex boundaries, the image area of the PIV recording can be divided into two regions: (1) region B contains particle images to be evaluated, whereas (2) region A covers particle images of other phases or disturbances resulting from background and flow boundaries. To separate the information of the two regions a mask $\Delta(i, j)$ is defined such that

$$\Delta(i, j) = \begin{cases} 0 & \text{if pixel } (i, j) \text{ belongs to region A} \\ 1 & \text{if pixel } (i, j) \text{ belongs to region B.} \end{cases} \quad (2)$$

Mask function $\Delta(i, j)$ can be considered as a binary image. If regions A and B are fixed during the PIV measurements and the boundary between the two regions is known, it is easy to 'draw' a mask for the PIV recordings. However, when the boundary between regions A and B varies from recording to recording, an automated identification of the boundary is necessary. Many algorithms for identifying objects in digital images have been described in the literature, e.g. Jähne (2002) and Gui (1998).

When mask $\Delta(i, j)$ is applied to the MQD method, the evaluation function is given as

$$D'(m, n) = \left\{ \sum_{i=1}^M \sum_{j=1}^N [g_1(i, j) - g_2(i + m, j + n)]^2 \times [\Delta_1(i, j) \Delta_2(i + m, j + n)] \right\} \times \left\{ \sum_{i=1}^M \sum_{j=1}^N \Delta_1(i, j) \Delta_2(i + m, j + n) \right\}^{-1} \quad (3)$$

where $\Delta_1(i, j)$ and $\Delta_2(i, j)$ are masks for the first and second recordings, respectively. A direct computation of $D'(m, n)$ requires considerable computer time. However, the FFT algorithm can be used to accelerate the computation of function $D'(m, n)$ with the following three steps.

Step 1. Multiply grey value distribution g_1 and g_2 with Δ_1 , Δ_2 :

$$g'_1(i, j) = g_1(i, j) \cdot \Delta_1(i, j) \quad (4)$$

$$g'_2(i, j) = g_2(i, j) \cdot \Delta_2(i, j). \quad (5)$$

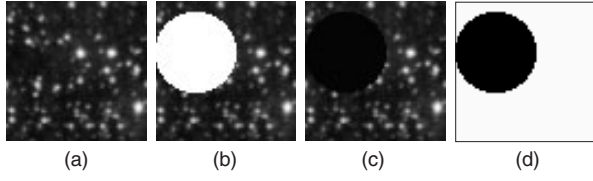


Figure 1. PIV samples: (a) original; (b) with a dispersed particle; (c) dispersed particle removed; (d) mask.

Step 2. Compute the following correlation functions using FFT:

$$C_1(m, n) = \sum_{i=1}^M \sum_{j=1}^N g_1^2(i, j) \cdot \Delta_2(i + m, j + n) \quad (6)$$

$$C_2(m, n) = \sum_{i=1}^M \sum_{j=1}^N g_1'(i, j) \cdot g_2'(i + m, j + n) \quad (7)$$

$$C_3(m, n) = \sum_{i=1}^M \sum_{j=1}^N \Delta_1(i, j) \cdot g_2^2(i + m, j + n) \quad (8)$$

$$C_4(m, n) = \sum_{i=1}^M \sum_{j=1}^N \Delta_1(i, j) \cdot \Delta_2(i + m, j + n). \quad (9)$$

Step 3. Compute evaluation function $D'(m, n)$ with

$$D'(m, n) = \frac{C_1(m, n) - 2C_2(m, n) + C_3(m, n)}{C_4(m, n)}. \quad (10)$$

Note that four correlation functions (i.e. C_1 , C_2 , C_3 and C_4) need to be computed to get evaluation function $D'(m, n)$, and that in step 2 a zero-padding technique is necessary to carry out the FFT computation (Gui and Merzkirch 2000), since g_2 and Δ_2 are not limited in the $(M \times N)$ -pixel window.

When the digital mask technique is applied to the correlation-based tracking algorithm, the evaluation function becomes

$$\begin{aligned} \Phi'(m, n) &= \frac{C_2(m, n)}{C_4(m, n)} \\ &= \frac{\sum_{i=1}^M \sum_{j=1}^N g_1'(i, j) \cdot g_2'(i + m, j + n)}{\sum_{i=1}^M \sum_{j=1}^N \Delta_1(i, j) \cdot \Delta_2(i + m, j + n)}. \end{aligned} \quad (11)$$

The correlation-tracking-based mask technique requires two correlation functions (C_3 and C_4) to be computed, so that its computation time is reduced to half of that of the MQD-based mask technique.

When g_2 and Δ_2 are specified in the $(M \times N)$ -pixel interrogation window and repeated periodically outside the window, equation (11) becomes the evaluation function of the masked, correlation-based interrogation algorithm. As described by Gui and Merzkirch (2000), because the computation window of the correlation-based interrogation algorithm is generally smaller than those of the MQD method and the correlation-based tracking algorithm, the computation time is further reduced.

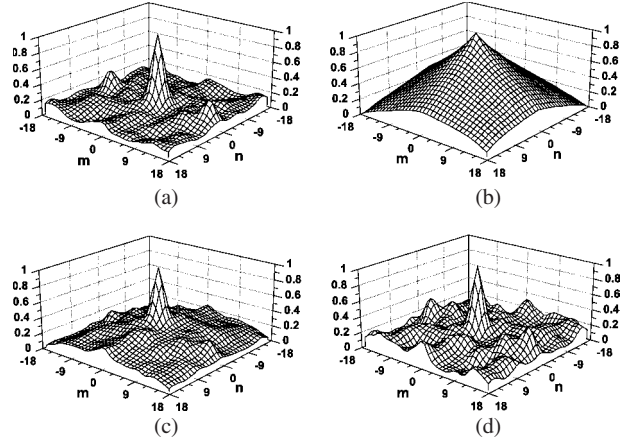


Figure 2. Correlation functions for (a) sample figure 1(a), (b) sample figure 1(b), (c) sample figure 1(c) and (d) sample figure 1(b) with mask figure 1(d).

2.2. Effect of the correlation-based digital mask

In order to evaluate the performance of the masked, correlation-based interrogation algorithm, a double-exposure PIV recording sample of 64×64 pixels, see figure 1(a), is used. The auto-correlation function of this PIV recording sample is shown in figure 2(a). The main correlation peak and the two symmetrically located secondary peaks can be seen clearly. The positions of two secondary correlation peaks, i.e. the possible particle displacements, are determined with the three-point Gaussian curve fit as $(14.29, -0.16)$ and $(-14.29, 0.16)$ in pixels.

In order to simulate the case of the two-phase flow, a large, round-shaped particle image, which does not move with the small tracer particles, is synthetically added to the PIV recording sample as shown in figure 1(b). The auto-correlation function of sample figure 1(b) is given in figure 2(b), in which the secondary correlation peaks that indicate the possible particle image displacements can no longer be identified. When the image of the big particle is removed from sample figure 1(b), and its area is padded with zeros (figure 1(c)), the two correlation peaks appear again at the positions of the possible particle image displacements; see figure 2(c). However, they are not the second highest peaks of the auto-correlation function. In this case the second highest peaks located at totally different positions, i.e. $(2.17, -6.87)$ and $(-2.17, 6.87)$ pixels. That means the influence of the big particle cannot be completely removed by simply erasing its image. When a mask (figure 1(d)) is used for separating the information of the two phases in the investigated sample figure 1(b), the displacement of the small tracer particles can be determined correctly again with equation (11) ($g_1 = g_2$, $\Delta_1 = \Delta_2$ for auto-correlation), because the influence of the big particle on the correlation function is minimized, and, consequently, the peaks resulting from the particle image displacement can be identified clearly (figure 2(d)). The possible particle image displacements determined with function figure 2(d), i.e. $(14.54, -0.12)$ or $(-14.54, 0.12)$ pixels, deviate slightly from those determined with function figure 2(a), because there are fewer tracer particle images in sample figure 1(b) than in sample figure 1(a).

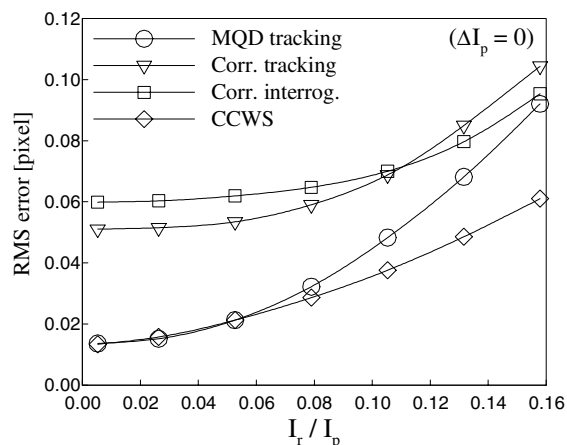


Figure 3. Influence of the random noise intensity on evaluation errors for four different algorithms.

2.3. Base algorithm of the mask technique

The above discussions show that the digital mask technique not only works on the basis of the MQD tracking method but can also be combined with the correlation schemes. The most commonly used correlation schemes are the correlation-based interrogation algorithm and the correlation-based tracking algorithm. For the former the correlated functions $g_1(i, j)$ and $g_2(i, j)$ are limited in the interrogation window of $M \times N$ pixels and assumed to be distributed periodically in the unbounded ij -plane, so that the FFT algorithm can be applied. For the latter $g_2(i, j)$ is defined in a larger area than $g_1(i, j)$, so that a zero-padding technique is necessary when the FFT is used for accelerating the computation. One of the latest advances of the correlation-based evaluation algorithm is the use of a continuous window shift. The correlation-based continuous window shift (CCWS) avoids the large bias error and strong peak-locking effect of the correlation-based interrogation algorithm. A detailed comparative study of the MQD tracking method, correlation-based tracking algorithm and correlation-based interrogation algorithm was presented by Gui and Merzkirch (2000) for ideal particle images. Some comparisons between the correlation-based tracking and the CCWS were conducted by Gui and Wereley (2002). The above-mentioned PIV evaluation algorithms are compared here again in the cases of single-pixel random noise and unequal illumination between the two images in a PIV recording pair.

In order to complete the comparison, synthetic PIV recording pairs are generated in the size of 1024×1024 pixels. 20480 particle images have a Gaussian grey value profile and are distributed randomly in the synthetic PIV recording, so that the particle image number density is 20 per 32×32 pixel window. The diameter and brightness (I_p) of the particle images vary randomly within 2–5 pixels and 130–250, respectively. First, the influence of the random noise intensity (I_r) on the root-mean-square (RMS) evaluation error of the particle displacement components is investigated. The intensity I_r is here the standard deviation of the single-pixel random noise from the mean value I_0 . The grey value in the synthetic PIV recordings is the root sum square (RSS) of the grey value of the particle images and the grey value of the random noise. A four-roll-mill flow (Wereley and Gui 2001,

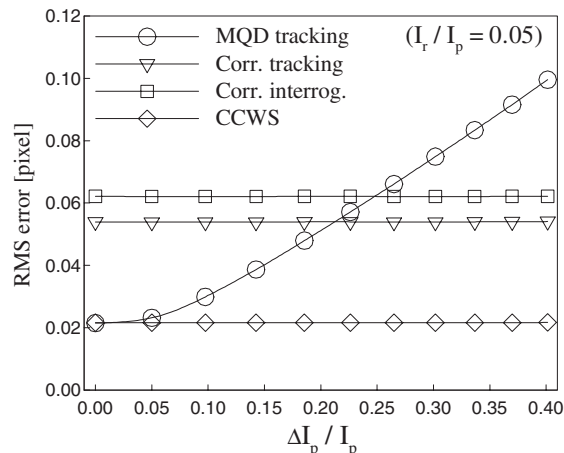


Figure 4. Influence of the unequal illumination between two PIV recordings in a pair on evaluation errors for four different algorithms.

2003) is simulated in these synthetic PIV recordings, so that the particle image displacement has a uniform distribution density in the region of $[-0.5, 0.5]$ pixels in both i and j directions. Seven pairs of synthetic PIV recordings are generated for the first test with I_r / I_p varying from 0 to 0.16. A 16×16 pixel grid system is chosen for the evaluations, so that 3969 interrogation points are distributed uniformly in the image plane. The seven synthetic PIV recording pairs are evaluated by using the MQD tracking method, the correlation-based tracking method (Corr. tracking), the correlation-based interrogation algorithm (Corr. interrog.) and the CCWS method with a 32×32 pixel interrogation window. For the CCWS five iterations are applied. The RMS errors are computed and shown in figure 3 as functions of the random noise intensity.

Figure 3 shows that the evaluation errors increase with increasing random noise intensity for all the four evaluation algorithms tested here. The evaluation errors of the MQD tracking and the correlation-based tracking are more sensitive to the random noise intensity than those of the correlation-based interrogation and the CCWS algorithm. In this test the MQD tracking method produces smaller error than the correlation-based tracking and correlation-based interrogation but larger error than the CCWS algorithm. The second test is to investigate the influence of the unequal illumination between the two PIV recordings in a pair. The synthetic PIV recording pair of $I_r / I_p = 0.05$ is chosen for the test. The grey value distribution of the second recording is multiplied by a factor smaller than unity, so that a brightness difference ΔI_p is created between the two recordings in this pair. The test results given in figure 4 show that the three correlation schemes are not sensitive to the brightness difference, whereas the MQD method is. When the brightness difference is relatively large, e.g. here $\Delta I_p / I_p > 25\%$, the evaluation error of the MQD method is larger than those of the correlation-based tracking and the correlation-based interrogation algorithm. The above two tests confirm that CCWS is the most accurate algorithm among the four. A further improvement of the CCWS method is the correlation-based CDIC algorithm, which combines the advantages of CDI and image correction, enabling high accuracy even when evaluating PIV recordings of complex flows (Wereley and Gui 2001, 2003). Since the particle image

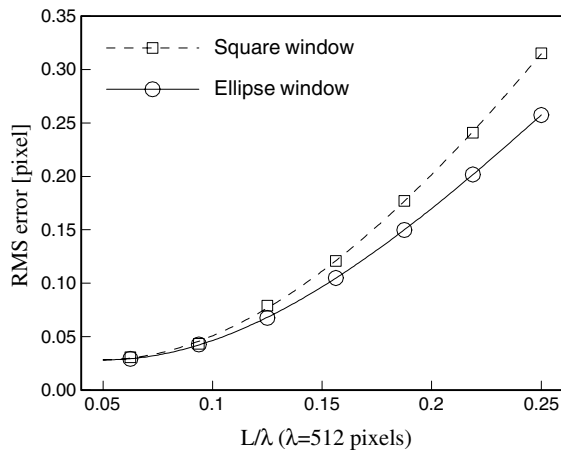


Figure 5. RMS errors for evaluating a complex flow using the CCWS algorithm with square and elliptical windows of different sizes (L : sidelength of the interrogation window, λ : wavelength of the periodical flow).

displacements used in these simulations are in the region of $[-0.5, 0.5]$ pixels, the particle image pattern deformation is very small. Consequently the differences between the CDIC and CCWS results cannot be seen with the scales used in figures 3 and 4.

Note that the statistical analyses in the above and following simulation tests were conducted with several thousand samples; the results are converged and repeatable.

2.4. Ellipse interrogation window

When evaluating digital PIV recordings, the interrogation window is usually chosen as a rectangular shape, so that the computation can be carried out easily. However, rectangular interrogation windows are apparently not optimal for resolving complex flows. To obtain a better resolution of complex flows with PIV, circular and elliptical interrogation windows were applied in some previous works. For example, Keane and Adrian (1992) considered circular interrogation spots and simple one-dimensional shear when deriving the recommended parameter space for cross-correlation PIV. They found that, for the most reliable results, the particle displacement gradient from one side of the interrogation window to the other should be smaller than 3% of the interrogation window diameter and simultaneously smaller than the particle image diameter. Translating these conditions to a flow with velocity gradients in both in-plane directions leads to generalization of the circular interrogation regions to elliptical ones, where the axis lengths are chosen according to the velocity gradients in each direction. In previous works, elliptical interrogation windows were formed either by using padding techniques or with window weighting functions. In the present work, an elliptical interrogation window is constructed with the mask technique, when the digital mask is defined as

$$\Delta(i, j) = \begin{cases} 1 & \text{for } \begin{cases} \text{pixel } (i, j) \text{ belongs to region B and} \\ \left(\frac{i - M/2}{M/2}\right)^2 + \left(\frac{j - N/2}{N/2}\right)^2 \leq 1 \end{cases} \\ 0 & \text{other.} \end{cases} \quad (12)$$

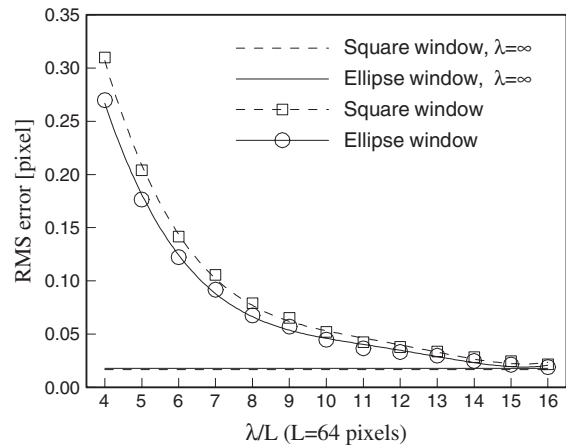


Figure 6. RMS errors for evaluating complex flows of different wavelengths using the correlation-based interrogation algorithm with a square and an elliptical window (L , sidelength of the interrogation window; λ , wavelength of the periodical flow).

In order to test the effect of the elliptical interrogation window, a synthetic PIV recording pair is generated with periodical distributed displacements, i.e. $S_x = A \cos(2\pi x/\lambda)$, $S_y = A \cos(2\pi y/\lambda)$. The number, brightness and size of the particle images are the same as those used in section 2.3. In this test the amplitude A and wavelength λ are 10 pixels and 512 pixels, respectively. This synthetic PIV recording pair is evaluated using the CCWS algorithm with seven different interrogation window sizes both with and without elliptical window masks. The test results in figure 5 show that a lower uncertainty level can be achieved for measuring complex flows, when the elliptical window mask is added to the CCWS algorithm, especially when the interrogation window is relatively large compared to flow gradients.

A further test is conducted with the 64×64 pixel interrogation window, while the wavelength varies to 16 times the interrogation window side length L ($=64$ pixels). The results given in figure 6 indicate that there are very large evaluation errors when using CCWS to evaluate PIV recordings of complex flows with high spatial frequency (short wavelength). An obvious improvement can be seen in figure 6, when the elliptical window is used with the CCWS algorithm. In this figure, the dashed and solid curves without symbols indicate the evaluation errors in the case of uniform flow, i.e. wavelength λ is infinitely ($\lambda = \infty$) large. In this ideal case the evaluation error without elliptical mask is slightly lower than that with elliptical mask, because the square window contains more pixels than the elliptical window.

Another comparison between the square and elliptical interrogation windows is conducted with more than 1000 PIV recording pairs taken in a wake flow of a flat plate with the xy -configuration of a towed PIV system. Details of this experiment were introduced by Gui *et al* (2001). The displacement of the particle images varies from 8 to 12 pixels in the main flow (x -) direction. A fixed window shift of 10 pixels is set for the evaluation, so that the magnitude of the particle image displacement to be determined is limited to 2 pixels in both x - and y -directions. This group of PIV recording pairs is first evaluated by using the correlation-based interrogation algorithm with a 32×32 pixel interrogation

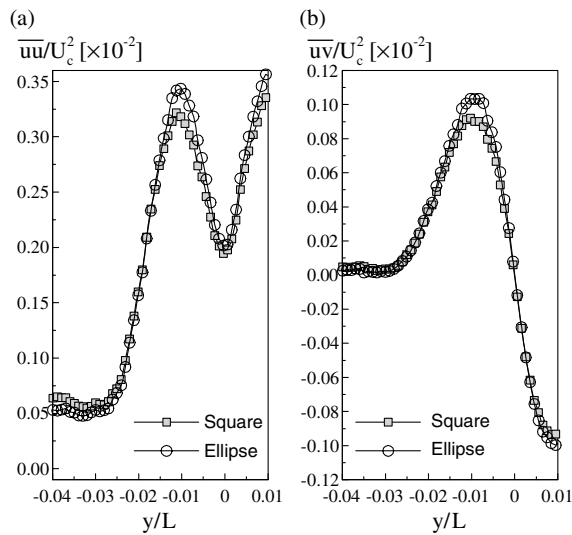


Figure 7. Normal (a) and shear (b) Reynolds stress distributions across the wake flow of a flat plate obtained by evaluating PIV recordings with correlation-based interrogation algorithm with and without elliptical window.

window and elliptical mask. Then a square window is applied with a smaller size (i.e. 30×30 pixels) so that the effective pixel number is the same as that of the ellipse window. After a statistical analysis of the evaluation results, normal and shear Reynolds stresses are determined. The distributions of the normal stresses in the x -direction and the shear stress in the xy -plane along a line at $x/L = 1.25$ are given in figure 7. It is shown that the normal and shear stress levels obtained with an elliptical window are obviously higher than those with a square window at the high turbulence centre ($y/L = -0.01$). A previous study (Gui *et al* 2001) indicates that the Reynolds stresses measured with the correlation-based interrogation window have lower magnitude than the real values because of the negative bias gradient. However, in the current test the increase of the Reynolds stress magnitude can be explained by the increased spatial resolution of the elliptical-shaped interrogation window in the high turbulence area. In figure 7(a) a lower normal stress is obtained with the elliptical window than the square window out of the wake region, i.e. $y/L < -0.025$. This implies that the elliptical window produces less error than the square window, because the measured normal stress is an RSS of the real normal stress and the evaluation error, and the real normal stress is very small in the uniform flow region, i.e. in the still water region of the towing tank.

3. Application examples

3.1. Solid-particle/water two-phase flow

In the first example, the correlation-based digital mask technique is applied in the measurement of the flow induced in a water tank by large solid buoyant particles released into the water at the bottom of the tank (Hilgers *et al* 1995). PIV recordings are taken consecutively with a CCD camera at a time interval $\Delta t = 20$ ms. The diameter of the tracer particle images is between 2 and 4 pixels, while the images of

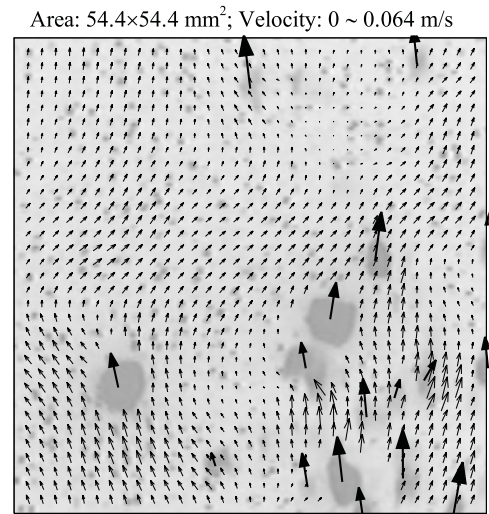


Figure 8. Example of the phase-separated evaluation of PIV recordings of a solid-particle/water two-phase flow: thin vectors for water flow; thick vectors for solid particles.

the solid buoyant particles are significantly bigger. A digital mask is constructed with image processing techniques for each recording to enable a phase-separated evaluation of the single-exposure two-phase PIV recording pairs. Figure 8 shows an overlapped velocity vector plot of the water (thin vectors) and the buoyant solid particles (thick vectors) in a measurement area of $54.4 \times 54.4 \text{ mm}^2$. The first recording of the evaluated PIV recording pair is presented as the background. The velocity field of the continuous phase (water) is evaluated using equation (11) in combination with the CDIC method and elliptical window mask. The based square window is 32×32 pixels, and the corresponding area is $6.4 \times 6.4 \text{ mm}^2$ in the flow. The velocity of the dispersed solid phase is evaluated with a particle-image-tracking algorithm. The velocity distribution of the water around the solid particles is well resolved because of the CDIC algorithm and elliptical window mask.

3.2. Bubbly water two-phase flow

The second application example of the correlation-based mask technique is the investigation of flow around an air bubble rising in water. A digital recording pair taken by a CCD camera with a time interval of 0.8 ms includes a bubble of roughly 7 mm in its long axis, which is released into the water at the bottom of a water tank. The experimental set-up and the PIV system were described in detail by Gui *et al* (1997) and Lindken *et al* (1999). The water flow is evaluated by using the correlation-based mask technique, CDIC algorithm and elliptical window mask, whereas the movement of the bubble is determined by identifying its edge. The relative flow field around the bubble is shown in figure 9. The interrogation window for the water flow is 32×32 pixels, that covers an area of $1.4 \times 1.4 \text{ mm}^2$ in the flow field. The flow structure of the water around the bubble is presented clearly in figure 9. As expected with a liquid-gas interface, the liquid velocity appears to ‘slip’ along the side surfaces of the bubble due to the great dynamic viscosity differences but is still seen to stagnate at the top and bottom of the bubble.

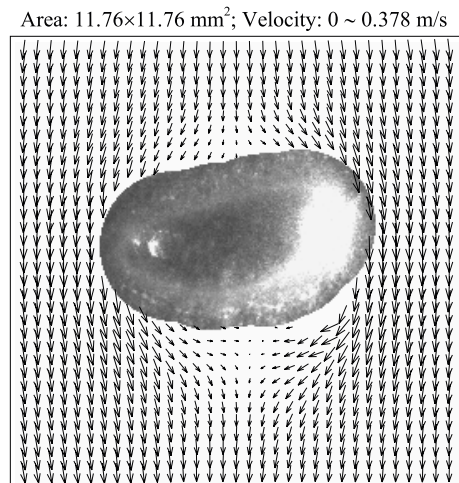


Figure 9. Example of the phase-separated evaluation of PIV recordings for a bubble/water flow (the velocity of the bubble is subtracted).

3.3. Flow around a human blood cell

This example will demonstrate that the digital mask technique can be applied not only to the phase-separated evaluation of two-phase PIV recordings, but also in the case of irregular flow boundaries. In a micro-PIV experiment a human red blood cell of about $9 \mu\text{m}$ in diameter is trapped between a coverslip and a slide glass held parallel $4 \mu\text{m}$ apart and surrounded by deionized, particle-seeded water (Wereley *et al* 1998). The flow is driven around the blood cell using the surface tension of a water drop placed at the edge of the coverslip. 50 PIV recordings are consecutively taken with a time interval of $\Delta t = 68.5 \text{ ms}$ to enable an average correlation function scheme with 49 recording pairs (Meinhart *et al* 2000). A mask of the blood cell image is constructed so that the flow near its surface can be determined. An interrogation window of 24×24 pixels is selected for the evaluation using the correlation-based digital mask technique with an elliptical window mask. The CDIC technique is applied in the evaluation to further reduce the measurement uncertainty. The evaluation results of this group of micro-PIV recordings are shown in figure 10 with the blood cell image in the background. In comparison with the evaluation results presented in an earlier work conducted by Wereley and Meinhart (2001) for the same blood cell, figure 10 provides a much better resolution of the water flow around the blood cell. The velocity field shown in figure 10 exhibits features that are expected from a Hele–Shaw flow. Far from the ‘cylinder’, the velocity field is uniformly directed upward and to the right at about a 75° angle from the horizontal. On either side of the red blood cell, there are stagnation points where the velocity goes to zero. The velocity field is symmetric with respect to reflection in a plane normal to the page and passing through the stagnation points. The velocity field differs from potential flow in that near the red blood cell there is evidence of the no-slip velocity condition, demonstrating the breakdown of Hele–Shaw flow very near the blood cell.

3.4. Flow around the tip of a vibrating cantilever

The most recent application of the correlation-based digital mask technique is in the measurement of flow induced

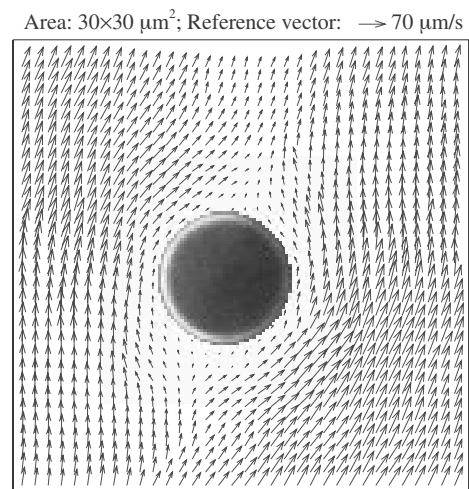


Figure 10. Water flow around a human blood cell.

by a vibrating cantilever, i.e. a piezoelectric fan. The miniaturization of electronic devices requires new techniques of cooling. Since the application of the conventional rotating blade type fans is limited by the size and complexity, new types of fans are expected to be developed to replace them in microscale convection-cooling systems. One of the alternatives is the piezoelectric fan, which has very simple structure and is easily miniaturized. It consists only of a cantilever plate and a piezoelectric material on the plate as a bending actuator. When alternating voltage is applied, the piezoelectric material generates cyclic bending moments and the cantilever plate vibrates. In order to evaluate the performance of the piezoelectric fan, experiments were conducted in the Micro Fluidics Laboratory at Purdue University with PIV (Kim *et al* 2003). The investigation was focused on the detailed flow field around a vibrating cantilever, which is 31 mm long and 38 mm wide. Two acrylic sidewalls are placed at each end of the cantilever to minimize the end effects of the cantilever. The vibrating frequency of the cantilever is set to 180 Hz , its natural frequency, and the peak-to-peak amplitude of the tip is 2.7 mm . A studio fog generator was used for particle seeding. The PIV imaging system is synchronized with the vibrating cantilever, so that a phase-averaged analysis can be conducted on the system. PIV recordings were taken with $\Delta t = 300 \mu\text{s}$ and a digital resolution of $15 \text{ pixels mm}^{-1}$. Figure 11 shows a PIV recording pair captured at phase angle $= 0$, i.e. the tip is undeflected and is moving from left to right. The viewed area in figure 11 is 200×400 pixels in the digital image and $13.3 \times 26.7 \text{ mm}^2$ in the flow field. The image of the cantilever tip can be seen clearly in both recordings of this pair and strong reflections are included in the first recording. In the experiment many recording pairs were collected for each selected phase to conduct a phase-averaged analysis.

In order to investigate the effect of the digital mask technique, the PIV recording pairs taken at zero phase angle—cantilever undeflected but moving from left to right at its maximum speed—were first evaluated with the CDIC method but without the mask technique. The mean velocity distribution is shown in figure 12. Very strong disturbances are observed in figure 12(a) because of the cantilever image and

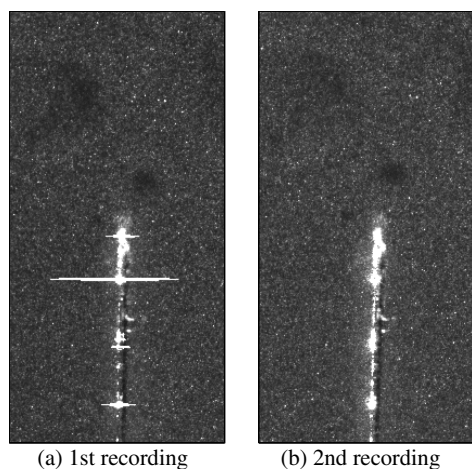


Figure 11. PIV recording pair taken at the tip of a vibrating cantilever (200×400 pixels/ 13.33×26.7 mm²).

the reflections. When the influence of the cantilever image and the reflections are ‘removed’ from the evaluation function by using the digital mask technique, a clear and reasonable flow pattern is obtained near the cantilever tip. Notice especially in figure 12(a) that the fifth column of vectors from the left spanning the height of the cantilever is weak and irregular compared to those vectors to the left or the right. Further notice that the vectors just above the tip of the cantilever in figure 12(a) are considerably different from those in figure 12(b). In both of these regions, the vectors in figure 12(b) display more continuous behaviour when compared with their neighbours. The digital mask technique has removed the very bright scattered light from the images, enabling a better measurement to be made. This test is conducted with a 64×64 pixel interrogation window and a 75% overlap.

4. Summary and conclusions

In the present work the MQD-based digital mask technique is accelerated by using the FFT algorithm, and modified so that the mask technique can be combined with the correlation-based evaluation schemes. A test based on a double-exposure digital PIV recording sample demonstrates that the mask technique is more effective than the zero-padding technique for the correlation-based interrogation algorithm to reduce the influence of an unexpected object in the PIV recording. An investigation with synthetic PIV recording pairs indicates that the recently developed continuous window shift technique makes the correlation-based interrogation algorithm more accurate than both the MQD tracking and correlation-based tracking method, and to be the best base algorithm for the digital mask technique. The correlation-based digital mask technique can easily be combined with the CDIC method to achieve even higher accuracy.

Two general applications of the digital masking were discussed in the present work, i.e. removing images of unexpected objects in the measurement area and creating elliptical interrogation windows. The unexpected objects include particle images of different phase and any other objects that may affect the evaluation results, regardless of whether they are smaller or larger than the interrogation

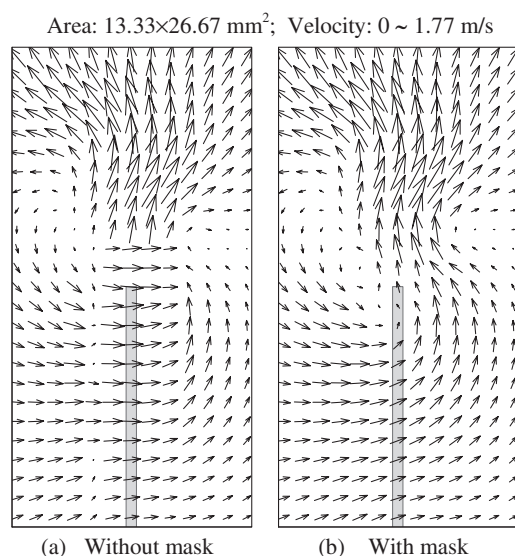


Figure 12. Mean velocity distribution evaluated without (a) and with (b) the digital mask technique.

window. The elliptical interrogation windows may be used to further increase the spatial resolution and accuracy of PIV measurements in complex and turbulent flows.

Applications in PIV measurements of solid/water two-phase flow, bubbly water flow, flow around a human blood cell and airflow near the tip of a vibrating cantilever verify the capability of the combined method of the digital mask technique, the elliptical interrogation window and the CDIC evaluation scheme.

Acknowledgment

This work was supported by the Indiana 21st Century Research and Technology Fund.

References

- Cowen E A and Monismith S G 1997 A hybrid digital particle tracking velocimetry technique *Exp. Fluids* **22** 199–211
- Gui L 1998 *Methodische Untersuchungen zur Auswertung von Aufnahmen der digital Particle Image Velocimetry* (Aachen: Shaker)
- Gui L, Lindken R and Merzkirch W 1997 Phase-separated PIV measurements of the flow around systems of bubbles rising in water *FEDSM'97: ASME Fluids Engineering Division Summer Mtg (June)*
- Gui L, Longo J and Stern F 2001 Biases of PIV measurement of turbulent flow and the masked correlation-based interrogation algorithm *Exp. Fluids* **30** 27–35
- Gui L and Merzkirch W 1996a Phase-separation of PIV measurements in two-phase flow by applying a digital mask technique *ERCOFTAC Bull.* **30** 45–8
- Gui L and Merzkirch W 1996b A method of tracking ensembles of particle images *Exp. Fluids* **21** 465–8
- Gui L and Merzkirch W 1997 A fast mask technique for the phase-separated evaluation of two phase PIV recordings *7th Int. Conf. on Laser Anemometry—Advances and Applications (Karlsruhe, Sept.)*
- Gui L and Merzkirch W 2000 A comparative study of the MQD method and several correlation-based PIV evaluation algorithms *Exp. Fluids* **28** 36–44

- Gui L, Merzkirch W and Lindken R 1998 An advanced MQD tracking algorithm for DPIV *9th Int. Symp. on Applications of Laser Techniques to Fluid Mechanics (Lisbon, July)*
- Gui L and Wereley S T 2002 A correlation-based continuous window shift technique for reducing the peak locking effect in digital PIV image evaluation *Exp. Fluids* **32** 506–17
- Hilgers S, Merzkirch W and Wagner T 1995 PIV measurements in multiphase flow using CCD- and photo-camera *ASME FED* **209** 151–4
- Huang H T, Fiedler H E and Wang J J 1993 Limitation and improvement of PIV: part II. Particle image distortion, a novel technique *Exp. Fluids* **15** 263–73
- Jähne B 2002 *Digital Image Processing* 5th revised and extended edn (Berlin: Springer)
- Keane R D and Adrian R J 1992 Theory of cross-correlation analysis of PIV images *Appl. Sci. Res.* **49** 191–215
- Keane R D and Adrian R J 1993 Theory and simulation of particle image velocimetry *5th Int. Conf. on Laser Anemometry—Advances and Applications (Veldhoven, Netherlands, Aug.) (Proc. SPIE)* vol 2052 (Bellingham, WA: SPIE Optical Engineering Press) pp 477–92
- Kim Y H, Wereley S T and Chun C H 2003 Phase-resolved flow field produced by a vibrating cantilever plate between two endplates *Phys. Fluids* submitted
- Lindken R, Gui L and Merzkirch W 1999 Velocity measurements in multiphase flow by means of particle image velocimetry *Chem. Eng. Technol.* **22** 202–6
- Lindken R and Merzkirch W 1999 Phase separated PIV and shadow-image measurements in bubbly two-phase flow *Proc. 8th Int. Conf. on Laser Anemometry—Advances and Applications* pp 165–71
- Lindken R and Merzkirch W 2000 Velocity measurements of liquid and gaseous phase for a system of bubbles rising in water *Exp. Fluids* **29** 194–201
- <http://link.springer.de/link/service/journals/00348/bibs/0029007/0029s194.htm>
- Meinhart C D, Wereley S T and Santiago J G 2000 A PIV algorithm for estimating time-averaged velocity fields *J. Fluids Eng.* **122** 285–9
- Merzkirch W, Gui L, Hilgers S, Lindken R and Wagner T 1997 PIV in multiphase flow *Proc. 2nd Int. Workshop on PIV'97 (Fukui)* pp 165–71
- Sholl M J and Savas Ö 1997 A fast Lagrangian PIV method for study of general high gradient flow *35th AIAA Aerospace Science Mtg (Reno, NV, Jan.) AIAA paper* 97-0493 (A97-15543)
- Sjödahl M 1994 Electronic speckle photography: increased accuracy by nonintegral pixel shift *Appl. Opt.* **33** 6667–73
- Wereley S T and Gui L 2001 PIV measurement in a four-roll-mill flow with a central difference image correction (CDIC) method *4th Int. Symp. on Particle Image Velocimetry (Göttingen, Sept.)*
- Wereley S T and Gui L 2003 A correlation-based central difference image correction (CDIC) method and application in a four-roll-mill flow PIV measurement *Exp. Fluids* **34** 42–51
- Wereley S T and Meinhart C D 2000 Accuracy improvements in particle image velocimetry *10th Int. Symp. on Applications of Laser Techniques to Fluid Mechanics (Lisbon, July)*
- Wereley S T and Meinhart C D 2001 Second-order accurate particle image velocimetry *Exp. Fluids* **31** 258–68
- Wereley S T, Meinhart C D, Santiago J G and Adrian R J 1998 Velocimetry for MEMS applications *Proc. ASME/DSC Micro-Fluidics Symp. (Anaheim, CA, Nov.)* vol 66 (New York: ASME) pp 453–9
- Westerweel J, Dabiri D and Gharib M 1997 The effect of a discrete window offset on the accuracy of cross-correlation analysis of digital PIV recordings *Exp. Fluids* **23** 20–8
- Willert C E 1996 The fully digital evaluation of photographic PIV recordings *Appl. Sci. Res.* **56** 79–102